Journal of Superconductivity and Novel Magnetism (2020) 33:877–882
https://doi.org/10.1007/s10948-019-05259-6

ORIGINAL PAPER

Magnetic Properties, Phase Transition Temperatures, Intergranular Exchange Interactions and Microstructure of Ta-Doped Nd-Ce-Fe-B Nano ribbons

Sajjad Ur Rehman[1] · Jie Song[1] · Qingzheng Jiang[1] · Lunke He[1] · Xie Weicheng[1] · Zhenchen Zhong[1]

Received: 30 April 2019 / Accepted: 12 August 2019 / Published online: 3 September 2019

Abstract
The effects of Ta doping on the magnetic properties, temperature stabilities, phase constituents, intergranular exchange interactions, and microstructures of $(Nd_{0.8}Ce_{0.2})_{13.5}Fe_{80.5-x}Ta_xB_6$ ($x = 0$–1.5) nanoribbons are investigated in this paper. It is found that Ta doping increased the coercivity of the alloys, while the remanence remained nearly unchanged. The temperature stability of the alloys improved significantly as the absolute value of temperature coefficient of coercivity β enhanced from 0.48%/K for Ta-free alloy to 0.38%/K for the alloys with 0.3–1.5 at.% Ta addition. The lattice constants (a, c), unit cell volume, and phase transition temperatures (T_{sr}, T_C) of the alloys changed by adding Ta into the alloys. Comprehensive best magnetic properties of $H_{cj} = 16.0$ kOe, $B_r = 7.65$ kG, and $(BH)_{max} = 12.60$ MGOe are obtained in $(Nd_{0.8}Ce_{0.2})_{13.5}Fe_{79.6}Ta_{0.9}B_6$ ribbon. The improvement in magnetic properties is mainly attributed to refined and uniform microstructure of the Ta-doped alloys.

Keywords NdCeFeB alloys · Ta doping · Magnetic materials · Exchange interaction · Microstructure

1 Introduction

Nd-Fe-B-based permanent magnetic materials have been extensively used in the last four decades as the strongest permanent magnets [1]. The ever increasing demand followed by supply restrictions of critical rare earth elements Nd, Pr, Dy, and Tb has resulted in large price fluctuations in the last few years [2]. Hence, the replacement of Nd/Pr by more abundant and low-cost RE elements such as Ce and La is widely studied in recent years. The partial replacement of Nd by abundant and economical element Ce has been suggested to reduce the cost of Nd-Fe-B-based permanent magnets [3, 4]. The intrinsic properties, i.e., saturation magnetization ($\mu_o M_s$) = 1.17 T, magnetocrystalline anisotropy (H_a) = 30 kOe, and Curie temperature (T_C) = 424 K of $Ce_2Fe_{14}B$ compound, are lower than the intrinsic properties $\mu_o M_s = 1.6$ T, H_a = 72 kOe, and $T_C = 585$ K of $Nd_2Fe_{14}B$ compound [5]. Thus, the extrinsic magnetic properties, intrinsic coercivity (H_{cj}), remanence (B_r), and maximum energy density $(BH)_{max}$ of CeFeB alloys are much lower than those of the NdFeB alloys [6, 7]. Some recent studies have reported that partial replacement of Nd by Ce would not decrease the magnetic properties of Nd-Fe-B-based magnets [8, 9]. The addition of Ce, however, decreases the thermal stability and T_C of the alloys due to low anisotropy field and low T_C of $Ce_2Fe_{14}B$ compound [10]. It is, therefore, technologically important to develop NdCeFeB-based magnets that could be used at elevated temperatures. One commonly used approach to improve the thermal stability of these type of alloys is to increase the T_C by partially substituting Co for Fe, but this type of substitution reduces the B_r and H_{cj} [3, 7]. Another approach to improve the thermal stability is to improve the H_a by heavy RE element substitution which ultimately reduces the B_r and $(BH)_{max}$ values due to antiferromagnetic coupling with Fe moments of RE elements [11]. The second approach for the improvement of magnetic properties is to improve the microstructure-dependent properties such as H_{cj}, B_r, and $(BH)_{max}$. Two types of dopant elements

✉ Zhenchen Zhong
zczhong2013@163.com

[1] Jiangxi Key Lab for Rare Earth Magnetic Materials and Devices/ Institute for Rare Earth Magnetic Materials and Devices, Jiangxi University of Science and Technology, Ganzhou, China

usually serve this purpose, i.e., low melting point elements and high melting point elements. The low melting point elements Al, Ga, Sn, and Cu modify the grain boundaries to decouple the main phase grains and improve the coercivity, but, as can be expected, the remanent magnetization of the alloys reduces [12, 13]. The high melting point elements Ti, Cr, W, V, Nb, Zr, and Mo refine the microstructure, form pinning center in the alloys, and partially or completely suppress the formation of deleterious α-Fe phase [14–20]. The H_{cj} of Nd-Fe-B ribbons is reported to increase as the nanograin size is reduced unless the alloys become amorphous, and the high melting point elements are very effective in reducing the grain size [21–23]. The high melting point elements are useful in improving the temperature stability of the Nd-Fe-B alloys [15–18]. The effects of Nb, Zr, Hf doping on magnetic properties and microstructure of Nd-Ce-Fe type alloys have been found beneficial for improving the magnetic properties of the alloys specifically at elevated temperatures [8, 15, 20].

Chin et al. [24] found that Ta addition to Nd-Dy-Fe-Co-B alloys improve the coercivity at room temperature while Liu et al. [25] found that Ta improves the room temperature properties of $Nd_9Fe_{86}B_5$ alloys. Furthermore, Ta has been applied to soft magnetic materials like Fe and Fe-Co for improving glass forming ability and thermal stability [26, 27]. In our recent work we found that Ta doping improves the H_{cj} values of Nd-Fe-B alloys without deteriorating the B_r values [27]. However, to the best of our knowledge no dedicated paper is available on Ta doping on Nd-Ce-Fe-B type alloys. In this paper we report the effects of Ta on the microstructure, magnetic properties, phase transition temperature and intergranular exchange interactions of $(Nd_{0.8}Ce_{0.2})_{13.5}Fe_{80.5-x}Ta_xB_6$ alloys. It is found that the addition of Ta refines the microstructure of the alloys and hence improves the magnetic properties significantly specifically at high temperatures. The reported magnetic properties in the current manuscript are better than the previous studies on Nd-Ce-Fe-B type alloys of near or same composition [8, 16, 21, 27].

2 Experimental Techniques

The precursor alloys, $(Nd_{0.8}Ce_{0.2})_{13.5}Fe_{80.5-x}B_6Ta_x$ (x = 0.0–1.5 at.%) were fabricated by melting pure elements (99.95%) in electric arc furnace five times under Ar. gas protection. The ingot fragments of about 7 g were loaded in quartz tube and were melt-spun onto Cu crucible rotating at angular speed 16 to 25 ms^{-1}. The quartz tube ejection nozzle and ejection pressure were kept constant at ~0.8 mm and 0.1 MPa, respectively. The Cu wheel was polished with fine scale grit paper to obtain smooth ribbons. The magnetic properties of the alloys were measured by applying magnetic field of 4.0 T in PPMS (Quantum Design, USA) equipped with VSM module. The crystal structures were characterized by using D8-advance (Bruker/AXS, Germany) X-ray diffractometer (XRD) using monochromatic Cu-K_α radiation. The XRD patterns were analyzed by applying Rietveld refinement in Rietica software. The low-temperature M-T curves were obtained in PPMS applying 0.1 T field in the temperature range 5–300 K. The Curie temperatures of the alloys were determined obtaining DSC curves in the temperature range 300–630 K. The nanostructures of selected alloys were analyzed and compared by using TEM (Tecnai G^2 F20).

3 Results and Discussion

The room temperature (RT) demagnetization curves of $(Nd_{0.8}Ce_{0.2})_{13.5}Fe_{80.5-x}Ta_xB_6$ ($x = 0.0$–1.5 at.%) alloys are depicted in Fig. 1a, while Fig. 1b displays the demagnetization curves of $(Nd_{0.8}Ce_{0.2})_{13.5}Fe_{80.5-x}Ta_xB_6$ alloys at 400 K. The coercivity (H_{cj}), remanence (B_r), and energy density $(BH)_{max}$ of Ta-free ribbons are 14.9 kOe, 7.64 kG, and 12.59 MGOe respectively, which are comparable or better than the B_r values reported previously [8, 15, 20]. The H_{cj} gradually and linearly increase from 14.9 kOe for standard alloy to 16.1 kOe for 1.2 at.% Ta. The remanent magnetization B_r remains nearly constant for 0.0 to 0.9% Ta, and decreases slightly for 1.2% Ta and further reduces for 1.5% Ta addition. This reduction in

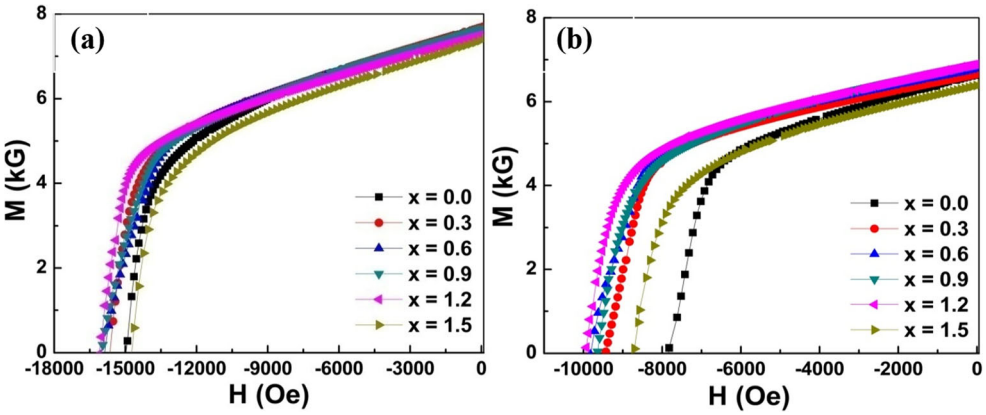

Fig. 1 Demagnetization curves of $(Nd_{0.8}Ce_{0.2})_{13.5}Fe_{80.5-x}Ta_xB_6$ alloys at 300 K (**a**) and 400 K (**b**)

Table 1 Temperature coefficients of $(Nd_{0.8}Ce_{0.2})_{13.5}Fe_{80.5-x}Ta_xB_6$ in the temperature range 300–400 K and lattice constants

x	α (%/K)	β (%/K)	a (Å)	c (Å)
0	−0.13	−0.48	8.781	12.175
0.3	−0.13	−0.40	8.783	12.179
0.6	−0.12	−0.38	8.784	12.185
0.9	−0.12	−0.39	8.785	12.189
1.2	−0.12	−0.38	8.787	12.191
1.5	−0.12	−0.39	8.787	12.192

magnetic properties might be due to the formation of nonmagnetic phases such as TaB and TaB_2 [28]. The $(BH)_{max}$ = 12.66 MGOe is obtained for $(Nd_{0.8}Ce_{0.2})_{13.5}Fe_{80.2}Ta_{0.3}B_6$ alloy. The best comprehensive magnetic properties of H_{cj} = 16.0 kOe, B_r = 7.65 kG, and $(BH)_{max}$ = 12.60 MGOe are obtained in $(Nd_{0.8}Ce_{0.2})_{13.5}Fe_{79.6}Ta_{0.9}B_6$ alloy. The H_{cj} values obtained in our current work are significantly higher than those obtained in our previous studies, while the B_r and $(BH)_{max}$ values are comparable with the previously obtained results [8, 15, 20]. All the alloys with or without Ta doping have quite high saturation remanence ratio of above 0.6 suggesting strong exchange coupling effect. To observe the effects of Ta doping on temperature stability, the *M-H* curves were obtained at 400 K. The demagnetization curves at 400 K are shown in Fig. 1b. The H_{cj} = 7.8 kOe, B_r = 6.63 kG, and $(BH)_{max}$ = 8.84 MGOe for the Ta-free sample are comparable with the values reported in the previous works [15, 20]. The H_{cj} at 400 K significantly improve with the addition of Ta into the alloys. The H_{cj} of all Ta-doped alloys are higher than the H_{cj} of Ta-free alloy. The room temperature of H_{cj} $(Nd_{0.8}Ce_{0.2})_{13.5}Fe_{79}Ta_{1.5}B_6$ is lower than that of $(Nd_{0.8}Ce_{0.2})_{13.5}Fe_{80.5}Ta_0B_6$ alloy, but significantly higher at 400 K which gives strong evidence that the temperature stability is improved by Ta doping. It is important to note that the magnetic properties were obtained at 300 K and at 400 K using the same samples. The best comprehensive magnetic properties H_{cj} = 9.95 kOe, B_r = 6.80 kG, and $(BH)_{max}$ = 9.90 MGOe at 400 K are obtained in $(Nd_{0.8}Ce_{0.2})_{13.5}Fe_{79.3}Ta_{1.2}B_6$ ribbons. These magnetic properties at 400 K are comparable with the magnetic properties of NdFeB ribbons without Ce substitution [4, 27]. The effect of Ta on the thermal stability of NdCeFeB type alloys is more prominent than that of Nb, Zr, and Hf [8, 15, 20].

The temperature coefficient of remanence (α) and temperature coefficient of coercivity (β) of the alloys were calculated by using the formulae $\alpha = \frac{B_r(T_1)-B_r(T_0)}{B_r(T_0)(T_1-T_0)} \times 100\%$ and $\beta = \frac{H_{cj}(T_1)-H_{cj}(T_0)}{H_{cj}(T_0)(T_1-T_0)} \times 100$ where T_1 = 400 K and T_o = 300 K. The α and β values of the investigated alloys are presented in Table 1. It can be seen that the temperature stability of the Ta-doped alloys is much better than the alloys without Ta doping.

The XRD patterns of $(Nd_{0.8}Ce_{0.2})_{13.5}Fe_{80.5-x}Ta_xB_6$ (x = 0–1.5 at.%) alloys are shown in Fig. 2. The major peaks have been identified and indexed. Rietveld refinement using Rietica software was applied to determine the lattice constants as depicted in Fig. 2b. The calculated lattice constants a and c of 2:14:1 phase are shown in Table 1. It can be noted that the lattice constants gradually increase with the addition of Ta indicating that some Ta may have entered into the main phase to substitute Fe sites. In addition to 2:14:1 phase, small amount of α-Fe was observed in XRD patterns which gradually decreased by adding Ta into the alloys. The α-Fe disappeared in the alloys containing ≥ 0.9 at.% Ta. Furthermore, the peaks slightly broaden and weaken with the addition of Ta which indicates that Ta doping reduces the grain size of the alloys. Chin et al. [24, 25] and Liu et al. [29] concluded that Ta and Ta-containing compounds can only be detected in XRD if they form large phases/inclusions. It is speculated on the basis of XRD results and TEM micrographs that Ta does not form large phases due to its small concentration, and hence could not be detected.

The spin reorientation temperature T_{sr} of RE-Fe-B-based magnets is an intrinsic property of the 2:14:1 phase that occurs due to a decrease of first-order anisotropy constant K_1 with

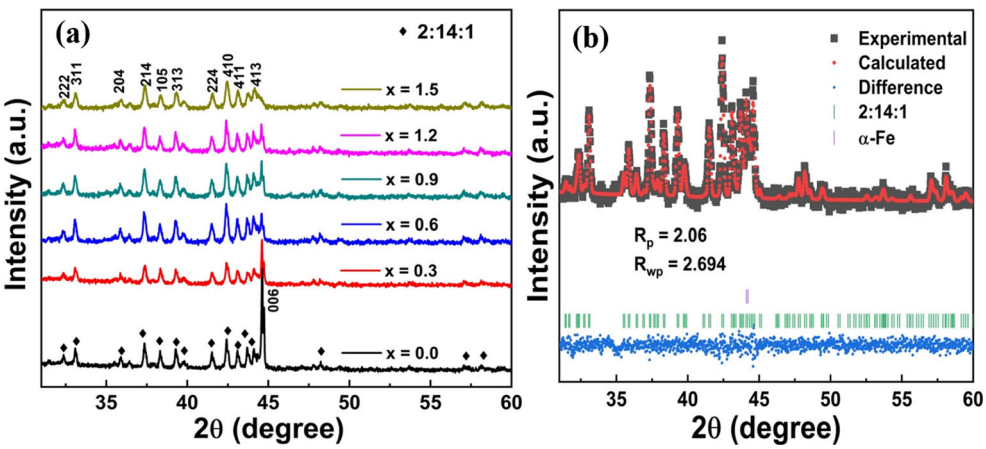

Fig.2 (**a**) XRD patterns of $(Nd_{0.8}Ce_{0.2})_{13.5}Fe_{80.5-x}Ta_xB_6$ ribbons and (**b**) the Rietveld refinement of the XRD pattern of $(Nd_{0.8}Ce_{0.2})_{13.5}Fe_{79.9}Ta_{0.6}B_6$ ribbon

decreasing T, and tilting from c-axis to the cone configuration with a cone angle of 30° at 4.2 K. The spin reorientation temperature of $Nd_2Fe_{14}B$ phase is reported to be 135 K [30]. The spin reorientation temperature disappears in $Ce_2Fe_{14}B$ phase [31, 32], thus making the $Ce_2Fe_{14}B$ phase more suitable for low-temperature applications. It is well known that T_{sr}, being an intrinsic property, changes when the composition of the main phase is altered [31]. The partial (20%) replacement of Nd by Ce reduces the spin reorientation temperature to 118 K (from 135 K for $Nd_2Fe_{14}B$), which further reduces as a result of Ta doping, and reaches 112 K for $(Nd_{0.8}Ce_{0.2})_{13.5}Fe_{79}Ta_{1.5}B_6$ alloy ribbon as shown in Fig. 3. The inset in Fig. 3 shows the dM/dT-T curve for $(Nd_{0.8}Ce_{0.2})_{13.5}Fe_{80.2}Ta_{0.3}B_6$ alloy. The low T_{sr} as a function of Ta doping indicates that some Ta enters into the NdCeFeB (2:14:1) main phase. Thus, the partial replacement of Ce for Nd and doping of Ta for Fe makes the alloys more suitable for low-temperature applications.

Another important intrinsic property of Nd-Fe-B type alloys is the Curie temperature (T_C). The T_C of $Nd_2Fe_{14}B$ compound depends on the strength of exchange interactions between Fe atoms. Any atom which enters into the 2:14:1 phase alters the Fe-Fe exchange interaction and ultimately changes the T_C. Therefore, elements like Ga are reported to increase the T_C by reducing the Fe-Fe distance and hence increasing the Fe-Fe interaction, and elements like Zr and Hf decrease the T_C by increasing the Fe-Fe distance and reducing their interaction [20, 33]. Figure 4 depicts the Curie temperature of $(Nd_{0.8}Ce_{0.2})_{13.5}Fe_{80.5-x}Ta_xB_6$ ($x = 0$–1.5) alloys. The T_C of $(Nd,Ce)_2Fe_{14}B$ is lower than the T_C of pure $Nd_2Fe_{14}B$ (~ 585 K), precisely because of the lower T_C of $Ce_2Fe_{14}B$ (~ 424 K). It is shown that the addition of Ta linearly decreases the T_C of the alloys which further confirms that Ta enters into the main phase and increases the distance between Fe-Fe atoms, ultimately reducing the Curie temperature of the alloys.

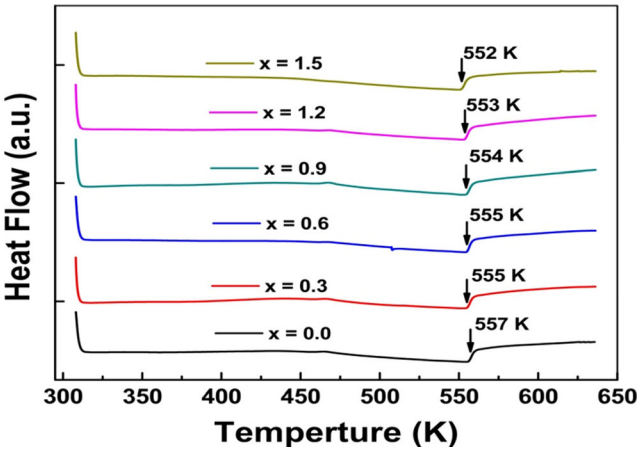

Fig. 4 DSC curves showing T_C of $(Nd_{0.8}Ce_{0.2})_{13.5}Fe_{80.5-x}Ta_xB_6$ ribbons

Intergranular exchange interactions via the magnetic moments at the grain interfaces are usually described by Henkel plot defined in mathematical equation as follows [34]:

$$\delta M\ (H) = [M_d(H) - M_r(\infty) + 2M_r(H)]/M_r(\infty) \quad (1)$$

where M_d (H) is the reduced magnetization and M_r (H) is the reduced remanent magnetization as a function of external field, and M_r (∞) is the remanent magnetization corresponding to the maximum applied external field [35]. The Henkel plots of $(Nd_{0.8}Ce_{0.2})_{13.5}Fe_{80.5-x}Ta_xB_6$ alloys plotted by using Eq. (1) are shown in Fig. 5. It can be seen that all plots have positive values which indicates strong intergranular exchange interaction [35]. The peaks of the plot slightly reduce as a function of Ta which indicates that some very small Ta-containing inclusions may reside at grain boundaries and reduce the intergranular interaction. There is a slight anomalous increase in the interaction for the best alloy ribbon, $(Nd_{0.8}Ce_{0.2})_{13.5}Fe_{79.6}Ta_{0.9}B_6$. This anomaly may be attributed to the more ideal microstructure which develops for the optimized Ta doping.

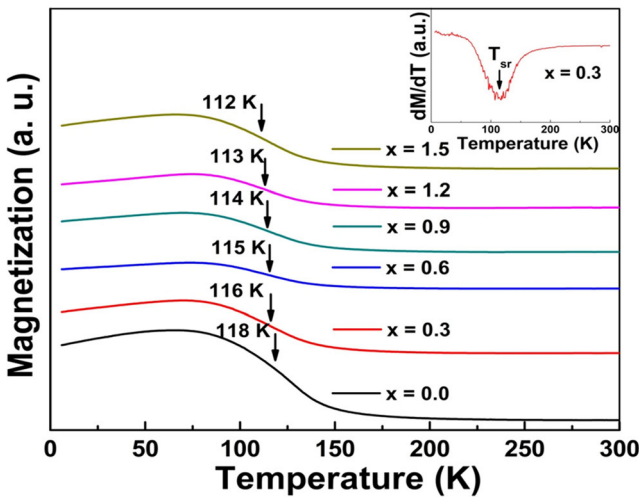

Fig. 3 M-T curves showing T_{sr} of $(Nd_{0.8}Ce_{0.2})_{13.5}Fe_{80.5-x}Ta_xB_6$ ribbons

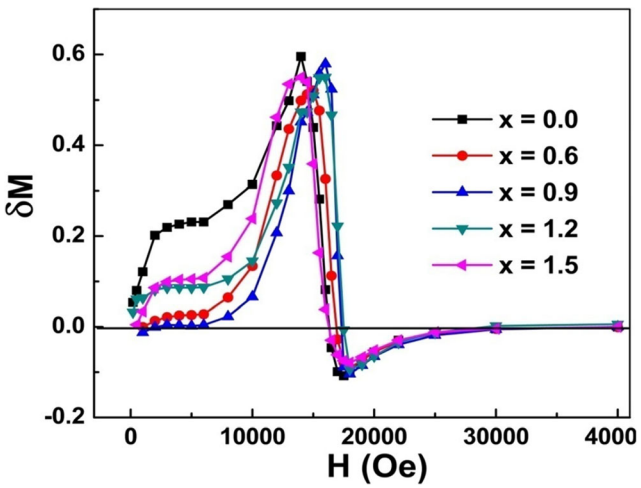

Fig. 5 Henkel plots of $(Nd_{0.8}Ce_{0.2})_{13.5}Fe_{80.5-x}Ta_xB_6$ ribbons

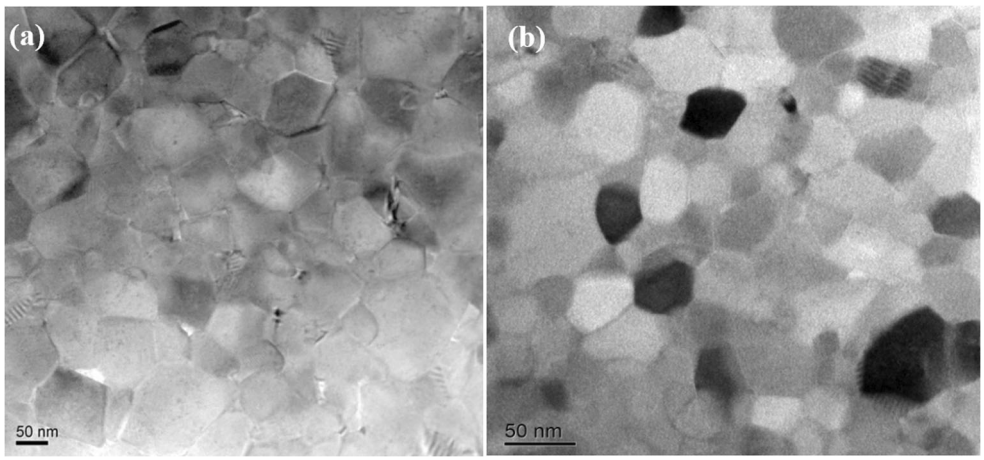

Fig. 6 TEM micrographs of $(Nd_{0.8}Ce_{0.2})_{13.5}Fe_{80.5-x}Ta_xB_6$ ribbons $x = 0.0$ (**a**) and $x = 0.9$ (**b**)

The room temperature superior magnetic properties of NdFeB type alloys mainly originate from intrinsic magnetic properties, i.e., high spontaneous magnetization and strong magnetocrystalline anisotropy. However, the extrinsic properties, H_{cj} and B_r and $(BH)_{max}$, largely depend on microstructure of the alloys. Refined microstructure is known to benefit the magnetic properties of the alloys [36, 37]. The transmission electron micrographs of the selected alloys are depicted in Fig. 6. The average grain size of the alloys without Ta doping is determined to be ~ 76 nm, while the alloy with 0.9 at.% Ta addition has an average grain size of ~ 40 nm. The grains below 250 nm behave as single domain [31], so the grains of the ribbons are well within the single domain limit. The addition of Ta has greatly reduced the grain size and has refined the grains by suppressing the formation of large grains as can be seen in Fig. 6b. The improved magnetic properties and thermal stabilities of the Ta-doped alloys are mainly attributed to the refined microstructure.

4 Conclusion

The effects of Ta doping on the magnetic properties, thermal stabilities, phase transition temperatures, intergranular exchange interactions, and microstructure were investigated. It is found that Ta doping enhanced the coercivity of the alloys. The coercivity of the alloys improved from 14.9 to 16.1 kOe, while the B_r reduced marginally. The addition of Ta greatly enhanced the thermal stability of the alloys. The overall improvement in magnetic properties by Ta doping is higher than the improvement obtained in our previous studies by Nb, Zr, and Hf substitution. All Ta-doped alloys depicted better H_{cj} values at elevated temperatures as compared with Ta-free alloy. The lattice parameters and phase transition temperatures of the alloys changed as a function of Ta indicating that some Ta atoms entered into the main phase to substitute Fe atoms. The average grains size of the alloys reduced as a result of Ta addition. The improved properties of the investigated alloys are mainly attributed to the refined and uniform microstructure. This work may be helpful in the development of Ce containing NdFeB-type alloys with improved magnetic properties and thermal stabilities.

Acknowledgments Sajjad Ur Rehman dedicates the paper to the memory of his father.

Funding Information This work was financially supported by the National Natural Science Foundation of China (Grant nos. 51564037, 51661011, and 51671097), the Outstanding PhD Dissertation Project (Grant no. 3105500032-Sajjad Ur Rehman), and Graduate Innovation Fund (Grant no. XS2018-B003-Sajjad Ur Rehman), Jiangxi University of Science and Technology, Ganzhou, China.

References

1. Zhao, L.Z., Zhang, J.S., Ahmad, G., Liao, X.F., Liu, Z.W., Greneche, J.M.: Sci. Rep. **8**(1), 6826 (2018)
2. Zhao, L.Z., Yu, H.Y., Guo, W.T., Zhang, J.S., Zhang, Z.Y., Hussain, M., Liu, Z.W., Greneche, J.M.: IEEE Trans Magn. **53**(11), 1 (2017)
3. Pathak, A.K., Khan, M., Gschneidner Jr., K.A., McCallum, R.W., Zhou, L., Sun, K., Dennis, K.W., Zhou, C., Pinkerton, F.E., Kramer, M.J., Pecharsky, V.K.: Adv. Mater. **27**, 2663 (2015)
4. Jiang, Q., Lei, W., He, L., Zeng, Q., Rehman, S.U., Zhang, L., Liu, R., Ma, S., Zhong, Z.: J. Alloys Compd. **775**, 449 (2019)
5. Herbst, J.F.: Mod Phys. **63**(63), 819 (1991)
6. Fan, X., Guo, S., Chen, K., Chen, R., Lee, D., You, C., Yan, A.: J. Magn. Magn. Mater. **419**, 394 (2016)
7. Rehman, S.U., Ouyang, H., Jiang, Q., Liu, K., He, L., Song, J., Wang, L., Luo, X., Ma, S., Zhong, Z.: J Magn Magn Mater. **486**, 165252 (2019)
8. Wang, L., Quan, Q., Zhang, L., Hu, X., Rehman, S.U., Jiang, Q., Du, J., Zhong, Z.: J. Appl. Phys. **123**, 113904 (2018)
9. Pei, K., Zhang, X., Lin, M., Yan, A.: J Magn Magn Mater. **398**, 96 (2016)
10. Jurczyk, M., Wallace, W.E.: J. Magn. Magn. Mater. **59**, L182 (1986)
11. Woodcock, T.G., Zhang, Y., Hrkac, G., Ciuta, G., Dempsey, N.M., Schrefl, T., Gutfleische, O., Givord, D.: Scr. Mater. **67**, 536 (2012)
12. Kurt Buschow, H.: Jürgen. Handb. Magn. Mater. **10**, 463 (1997)
13. Kim, A.S., Camp, F.E.: J. Appl. Phys. **79**, 5035 (1996)

14. Sagawa, M., Tenaud, P., Vial, F., Hiraga, K.: IEEE Trans. Magn. **26**, 1957 (1990)
15. Quan, Q., Zhang, L., Jiang, Q.Z., Lei, W., Zeng, Q., Hu, X., Wang, L., Yu, X., Du, J., Fu, G., Liu, R., Zhong, M., Zhong, Z.C.: J. Magn. Magn. Mater. **442**, 377 (2017)
16. Raviprasad, K., Ravishankar, N., Chattopadhyay, K., Umemoto, U.: J. Appl. Phys. **83**, 1916 (1998)
17. Hirosawa, S., Tomizawa, H., Mono, S., Hamamura, A.: IEEE Trans Magn. **26**, 1660 (1990)
18. Zhang, P.Y., Hiergeist, R., Albrecht, M., Braun, K.F., Sievers, S., Ludke, J., Ge, H.L.: J. Appl. Phys. **106**, 073904 (2009)
19. Leonowicz, M.: J. Magn. Magn. Mater. **83**, 211 (1990)
20. Zhang, L., Jiang, Q., Wang, L., Quan, Q., Rehman, S.U., Lei, W., He, L., Zeng, Q., Hu, X., Liu, R., Zhong, Z.: J. Magn. Magn. Mater. **474**, 305 (2019)
21. Pollard, R.J., Parker, S.F.H., Grundy, P.J.: J. Magn. Magn. Mater. **75**, 239 (1988)
22. Zhang, M., Li, Z., Shen, B., Hu, F.: J Sun J Alloys Compd. **651**, 144 (2015)
23. Chang, W.C., Wu, S.H., Ma, B.M., Bounds, C.O.: J. Magn. Magn. Mater. **167**, 65 (1997)
24. Chin, T.S., Lin, C.H., Huang, Y.H., Yau, J.M.: IEEE Trans. Magn. **29**, 2788 (1993)
25. Chin, T.S., Huang, S.H., Yau, J.M.: Appl. Phys. Lett. **59**, 2046 (1991)
26. Bekker, V., Seemann, K., Leiste, H., Magn, J.: Magn Mater. **296**, 37 (2006)
27. Liu, Z.W., Liu, Y., Yan, L., Tan, C.Y., Ong, C.K.: J. Appl. Phys. **99**, 043903 (2006)
28. Rehman, S.U., Jiang, Q., Lei, W., Zeng, L., Tan, Q., Ghanzanfar, M., Awan, S.U., Ahmad, T., Zhong, M., Zhong, Z.C.: J. Phys. Chem. Solids. **124**, 261 (2019)
29. Liu, Z.W., Liu, Y., Deheri, P.K., Ramanujan, R.V., Davies, H.A.: J. Magn. Magn. Mater. **321**, 2290 (2009)
30. Zhang, J.S., Li, W., Liao, X.F., Yu, H.Y., Zhao, L.Z., Zeng, H.X., Peng, D.R., Liu, Z.W.: Journal of mater. For. Sci. Technol. **35**, 1877 (2019). https://doi.org/10.1016/j.jmst.2019.05.007
31. Chui, W.B., Takashashi, Y.K., Hono, K.: Acta Mater. **59**, 7768 (2011)
32. Pathak, A.K., Khan, M., Gschneidner Jr., K.A., McCallum, R.W., Zhou, L., Sun, K., Kramer, M.J., Pecharsky, V.K.: Acta Mater. **103**, 211 (2016)
33. Rehman, S.U., Jiang, Q., Liu, K., He, L., Ouyang, H., Zhang, L., Wang, L., Ma, S., Zhong, Z.C.: J. Phys. Chem. Solids. **132**, 182 (2019)
34. Ashfaq, A., Matsuura, M., Sakurai, M.: Appl. Phys. Lett. **73**(17), 2512 (1998)
35. Kelly, P.E., O'Grady, K., Mayo, P.I., Chantrell, R.W.: IEEE Trans Magn. **25**, 3881 (1989)
36. Wohlfarth, E.P.: J. Appl. Phys. **29**(3), 595 (1958)
37. Jiang, Q., Zhong, M., Quan, Q., Zhang, J., Zhong, Z.C.: J Alloys Compd. **688**, 363 (2016)